Struct Multidisc Optim (2007) 33: 113–129
DOI 10.1007/s00158-005-0602-5

RESEARCH PAPER

C. Graczykowski · T. Lewiński

Michell cantilevers constructed within trapezoidal domains

Part IV: Complete exact solutions of selected optimal designs and their approximations by trusses of finite number of joints

Received: 13 May 2005 / Revised manuscript received: 20 September 2005 / Published online: 10 June 2006

Abstract The paper concerns the Michell-like cantilevers transmitting a point load to a straight segment of a support. The feasible domain is of trapezoidal infinite shape, as in the previous parts of the paper. The ratio of allowable stresses in tension and compression is arbitrary, not necessarily equal to 1. The present, last part of the paper includes detailed geometric and static analyses of the optimal cantilevers for various admissible data, thus providing new benchmarks of topology optimization. All results are found by using analytical methods developed in the previous parts of the paper. Particular attention is put on the force field distribution within the fibrous domains. These force fields turn out to be defined in certain subdomains forming a static division. The volumes of the optimal cantilevers are computed in two manners: by direct integration of the density of fibres and summing it up with the volume of the reinforcing bars of finite cross sections, and by using the kinematic formula of Michell according to which the volume is proportional to the virtual work. The examples analysed prove that both approaches lead to identical results of the volumes, thus showing that the possible duality gaps vanish. The analytical solutions are verified by considering appropriately chosen sequences of trusses of finite number of joints converging to the exact Michell cantilevers.

1 Introduction

Like in the limit load theory of structures, where two methods of assessing the limit load, static and kinematic, should provide the same limit load, any Michell-like solution is viewed as correct if both the primal (see (I.2.8)[1]) and dual (see (I.2.12)) formulae for the weight of the optimal cantilever yield exactly the same results. Usually, the latter formula is used in the literature because it requires only the knowledge of the virtual displacement fields. Finding this field is usually easier than finding the force fields involved in (I.2.8). In fact, the force fields depend heavily on the position of the point load, while the virtual displacement field is independent of the loading. Moreover, (I.2.8) involves integration, while (I.2.12) is algebraic, at least in the considered case of point loads. Even in the relatively simpler (than considered here) case of the Michell cantilever supported on a circle, the integration in (I.2.8) turns out to be fairly difficult and has been analytically performed only recently, see Graczykowski and Lewiński (2005). Nevertheless, any Michell solution should be checked by both formulae (I.2.8 and I2.12) to be sure that the solution is valid. Despite this obvious requirement called vanishing of the *duality gap*, this verification is remarkably rare in the literature; some simplest plane structures were verified in Hemp (1973), the cantilever supported on the circle has been verified by the present authors as noted above and the Michell sphere and other surfaces of revolution have been verified in Hemp (1973) and Lewiński (2004). Let us nonetheless note that neither of Chan-like solutions of the plane cantilevers supported on a straight segment reported in Hemp (1973), Chan (1967) and Lewiński et al. (1994a,b) have been verified till now. One of the aims of the present paper is to fill up this gap in the literature. The verification could not always have been done analytically, yet a numerical verification is reported in all the cases.

The present paper makes use of the geometric, kinematic and static results reported in the previous parts of the work. Knowledge of distribution of the Lamé coefficients A, B, of the force fields T_1, T_2 and of the longitudinal forces in the reinforcing bars makes it possible to determine the density of fibres function h, integration of which gives the volume of the material used for construction of the fibrous parts of the optimal cantilevers.

C. Graczykowski (✉)
Institute of Fundamental Technological Research,
Polish Academy of Sciences, Świętokrzyska 21, 00-049,
Warsaw, Poland
e-mail: Cezary.Graczykowski@ippt.gov.pl

T. Lewiński
Institute of Structural Mechanics, Faculty of Civil Engineering,
Warsaw University of Technology, al.Armii Ludowej 16,
00-637, Warsaw, Poland
e-mail: T.Lewinski@il.pw.edu.pl

[1] Equations of the previous parts of this paper (see Graczykowski and Lewiński 2006a,b,c), are referred to with Roman numerals (see conventions adopted in the Introductions to parts I and II).

We note that by (III.2.2),

$$|N_I| = T_1 \big/ B, \quad |N_{II}| = -T_2 \big/ A, \tag{1.1}$$

since $T_1 > 0$ and $T_2 < 0$, and by (I.2.13), the density function should be computed by

$$h(\alpha, \beta) = \frac{T_1(\alpha, \beta)}{\sigma_T B(\alpha, \beta)} - \frac{T_2(\alpha, \beta)}{\sigma_C A(\alpha, \beta)}. \tag{1.2}$$

The volume of the material used for the reinforcing bars is computed by appropriate line integrals. The total volume is found by summing up the volumes of the material used for constructing the bars and the fibrous domains. Obviously, the volume found should not be misinterpreted as a volume of the domain occupied by the structure; nevertheless, for the sake of brevity, the shorter notion, the volume of the structure, will also be used sometimes. The selected solutions are verified by comparing the exact results with those corresponding to sequences of trusses (of finite number of joints) tending to the exact solutions. This verification method has been used already by Prager (1978a,b) and is used here for more complicated layouts. It turned out that the exact results compare favorably with those results for approximating trusses. Lastly, let us mention that the problems discussed in the present paper have been recently analysed by Gilbert et al. (2005) by new, highly advanced numerical techniques.

The examples reported can serve as benchmarks of topology optimization software. That is why not only the essential information but some particular, technical results will also be given to make the benchmarks complete. The conventions of notation and references adopted in parts I–III apply here.

2 Prager–Hill cantilevers

If the point load is applied within the domain ABDC in Fig. I.10, an optimal cantilever is composed of two fans, Prager–Hill region ABDC and of two reinforcing bars (see sections I.6, II.5 and III.5. The aim of this section is to find the volume of such cantilevers by summing up the volumes of their parts, or by (I.2.8), and then verify this result by computing the virtual work using (I.2.12).

The density h of the fibres (see (I.2.13)) will be found by the formulae of sections I.6 and III.5. The density of fibres in the Hill–Prager domain ABDC is expressed by (1.2), with the force fields given by (III.5.5b and 5.6), and A,B given by (I.6.7 and I.6.8):

$$\begin{aligned} h(\alpha, \beta) = &\frac{-F_C G_0(\alpha_p - \alpha, \beta_p - \beta) + F_T G_1(\alpha_p - \alpha, \beta_p - \beta)}{\sigma_T [r_2 G_0(\beta, \alpha) + r_1 G_1(\alpha, \beta)]} \\ &- \frac{-F_T G_0(\alpha_p - \alpha, \beta_p - \beta) + F_C G_1(\beta_p - \beta, \alpha_p - \alpha)}{\sigma_C [r_1 G_0(\alpha, \beta) + r_2 G_1(\beta, \alpha)]}, \end{aligned} \tag{2.1}$$

where $F_C = F_C$ (P), $F_T = F_T$ (P) (see (III.5.1)) and $r_2 = \kappa^{1/2} r_1$ (see (I.4.10)).

In the lower circular fan we have (see (I.5.4) and (III.5.7))

$$h(\alpha, \beta_1) = -\frac{T_2}{\sigma_C A} = -\frac{-F_T G_0(\alpha_p - \alpha, \beta_p) + F_C G_1(\beta_p, \alpha_p - \alpha)}{\sigma_C r_1 \beta_1} \tag{2.2}$$

In the upper circular fan we have (see (I.5.2) and (III.5.8))

$$\begin{aligned} h(\alpha_1, \beta) &= \frac{T_1}{\sigma_T B} \\ &= \frac{-F_C G_0(\alpha_p, \beta_p - \beta) + F_T G_1(\alpha_p, \beta_p - \beta)}{\sigma_T r_2 \alpha_1}. \end{aligned} \tag{2.3}$$

Let us compute the volume of fibres and bars of the particular parts of the cantilever. The volume of fibres of the Hill–Prager domain (ABDC) is subsequently computed as follows:

$$V_{ABDC} = \int_0^{\alpha_p} \int_0^{\beta_p} h(\alpha, \beta) A(\alpha, \beta) B(\alpha, \beta) d\alpha d\beta$$

or

$$\begin{aligned} V_{ABDC} = &\frac{1}{\sigma_T} \int_0^{\alpha_p} \int_0^{\beta_p} \big[-F_C G_0(\alpha_p - \alpha, \beta_p - \beta) \\ &+ F_T G_1(\alpha_p - \alpha, \beta_p - \beta)\big] \\ &\cdot [r_1 G_0(\alpha, \beta) + r_2 G_1(\beta, \alpha)] d\alpha d\beta \\ &+ \frac{1}{\sigma_C} \int_0^{\alpha_p} \int_0^{\beta_p} \big[F_T G_0(\alpha_p - \alpha, \beta_p - \beta) \\ &- F_C G_1(\beta_p - \beta, \alpha_p - \alpha)\big] \\ &\cdot [r_2 G_0(\alpha, \beta) + r_1 G_1(\alpha, \beta)] d\alpha d\beta \end{aligned} \tag{2.4}$$

The integrals above can be expressed in terms of Lommel functions by using (a.31–a.36)[2] (I.A.6), which results in

$$V_{ABDC} = \frac{F_T}{\sigma_T}\left\{\beta_p\ (1+\kappa)\left[r_1 G_2(\alpha_p,\beta_p) + r_2 G_1(\alpha_p,\beta_p)\right] + r_2\ \left[1 - G_0(\alpha_p,\beta_p)\right]\right\}$$
$$+\left(\frac{-F_C}{\sigma_T}\right)\left\{\alpha_p(1+\kappa)\left[r_2 G_2(\beta_p,\alpha_p) + r_1 G_1(\beta_p,\alpha_p)\right] + r_1\kappa\left[1 - G_0(\alpha_p,\beta_p)\right]\right\}. \quad (2.5)$$

The volume of fibres in the lower circular domain NAC is subsequently computed using (a.4) as follows:

$$V_{NAC} = \int_0^{\alpha_p}\int_0^1 -\left(\frac{T_2}{\sigma_C}B\right)d\alpha d\beta_1$$
$$= \frac{F_T r_1}{\sigma_C}\int_0^{\alpha_p}\int_0^1 G_0(\alpha_p - \alpha, \beta_p)d\alpha d\beta_1$$
$$-\frac{F_C r_1}{\sigma_C}\int_0^{\alpha_p}\int_0^1 G_1(\beta_p, \alpha_p - \alpha)d\alpha d\beta_1$$
$$= \frac{1}{\sigma_T}\left(\kappa\cdot F_T r_1 G_1(\alpha_p,\beta_p) + \kappa F_C r_1 - \kappa F_C G_0(\beta_p,\alpha_p)\right). \quad (2.6)$$

The volume of fibres in the upper circular domain RBA is similarly computed with using (a.4) as follows:

$$V_{RBA} = \int_0^{\beta_p}\int_0^1 \left(\frac{T_1}{\sigma_T}A\right)d\alpha_1 d\beta$$
$$= \frac{-F_C r_2}{\sigma_T}\int_0^{\beta_p}\int_0^1 G_0(\alpha_p, \beta_p - \beta)d\alpha_1 d\beta$$
$$+\frac{F_T r_2}{\sigma_T}\int_0^{\beta_p}\int_0^1 G_1(\alpha_p, \beta_p - \beta)d\alpha_1 d\beta$$
$$= \frac{1}{\sigma_T}\left(-F_C r_2 G_1(\beta_p,\alpha_p) - F_T r_2 + F_T r_2 G_0(\alpha_p,\beta_p)\right). \quad (2.7)$$

The volume of the tension-reinforcing bar equals:

$$V_T = \frac{F_T}{\sigma_T}\left(\int_0^{\alpha_p} A(\alpha,\beta_p)d\alpha + r_2\right), \quad (2.8a)$$

where $A(\alpha, \beta_p)$ is given by (I.6.7). Integration gives

$$V_T = \frac{F_T}{\sigma_T}\left(r_1 G_1(\alpha_p,\beta_p) + r_2 G_0(\beta_p,\alpha_p)\right). \quad (2.8b)$$

[2] Equations (a.31–a.36) mean (31–36) in Lewiński et al. (1994a).

In a similar way, we compute the volume of the compression-reinforcing bar

$$V_C = -\frac{F_C}{\sigma_C}\left(\int_0^{\beta_p} B(\alpha_p,\beta)d\beta + r_1\right) \quad (2.9a)$$

and find

$$V_C = -\frac{\kappa\cdot F_C}{\sigma_T}\left(r_2 G_1(\beta_p,\alpha_p) + r_1 G_0(\alpha_p,\beta_p)\right). \quad (2.9b)$$

The sum of the volumes of the material used in all the parts of the cantilevers is expressed as

$$V = \frac{F_T}{\sigma_T}\cdot\left[\left(r_2 + (\kappa+1)r_1\alpha_p\right)\cdot G_0(\alpha_p,\beta_p)\right.$$
$$\left. + \alpha_p(\kappa+1)r_2 G_1(\beta_p,\alpha_p)\right]$$
$$-\frac{F_C}{\sigma_T}\cdot\left[\left(\kappa r_1 + (\kappa+1)\beta_p r_2\right)G_0(\beta_p,\alpha_p)\right.$$
$$\left. + (\kappa+1)\beta_p r_1 G_1(\beta_p,\alpha_p)\right]. \quad (2.10)$$

By using (II.5.11 and II.5.6) for the virtual displacements at the node of application of the point load, one can rearrange the formula above as follows:

$$V = \frac{F_T}{\sigma_T}\cdot u(\alpha_p,\beta_p) + \frac{F_C}{\sigma_T}\cdot v(\alpha_p,\beta_p). \quad (2.11a)$$

Substitution of (III.5.1) gives

$$V = \frac{P}{\sigma_T}\cdot\left[u(\alpha_p,\beta_p)\sin(\psi+\varphi) - v(\alpha_p,\beta_p)\cos(\psi+\varphi)\right]. \quad (2.11b)$$

We note that the expression (2.11b) has the meaning of the virtual work given by (I.2.12). Thus, both (I.2.12) and (I.2.8) give the same results. We conclude that the duality gap vanishes. The equivalence of both formulae proves that all the results concerning geometry of fibres, Lamé coefficients, virtual displacements, forces in the reinforcing bars and the forces within the fibrous domain are correct.

Let us look more closely at selected examples. Their analyses will include computation of volumes of the material used (weights) of all their parts, graphs of the density of fibres function h and force fields within the designs.

Example 2.1 Consider the problem of Fig. 1 for the case of κ=1. Then we write σ_T=σ_C=σ. The force **P** is directed such

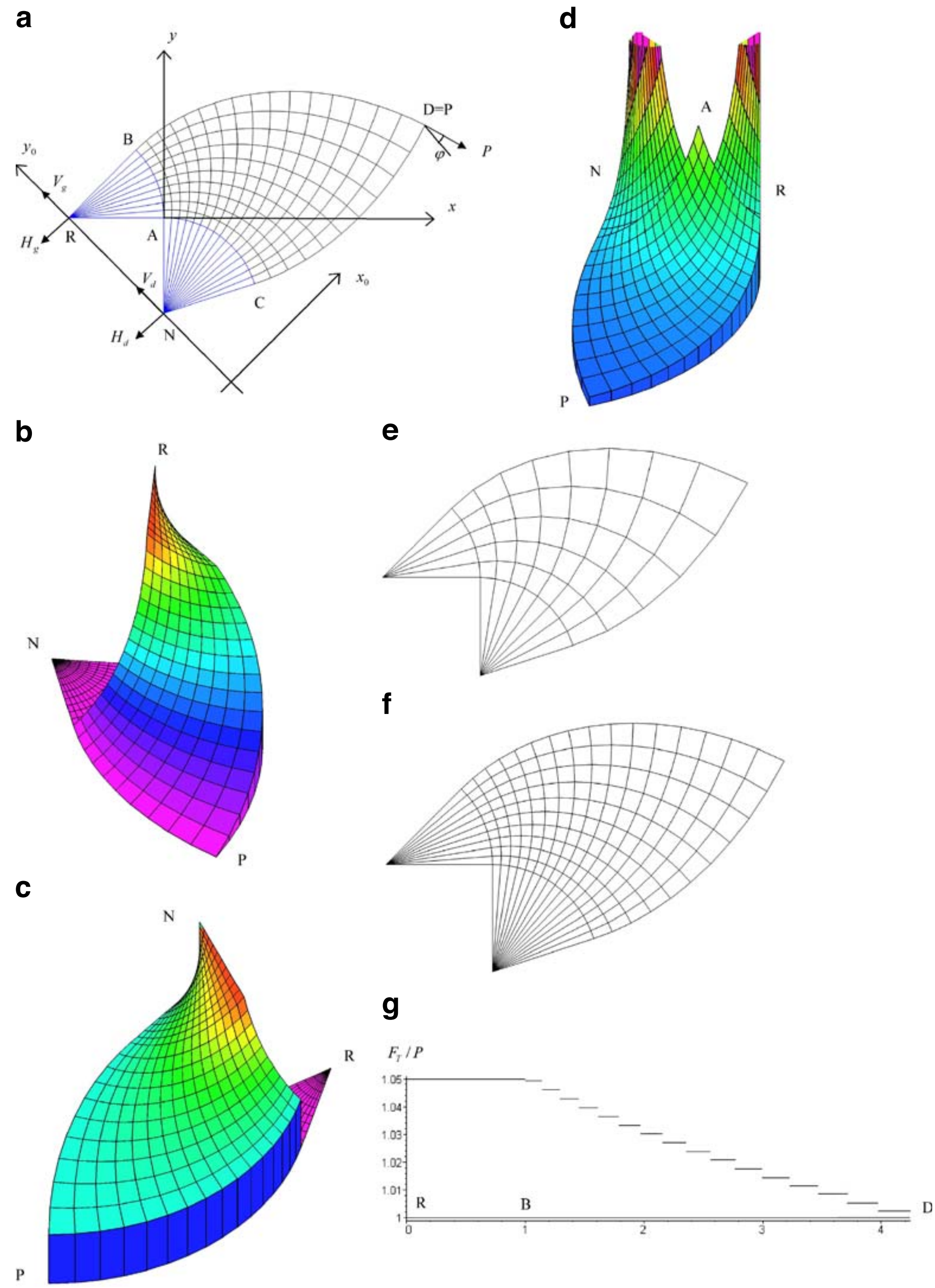

Fig. 1 **a** The first structure. The force **P** is tangent at D=P to the BD bar; **b** The plot of the force field T_1; **c** The plot of the force field T_2; **d** The plot of the density function h. The values of the non-dimensional quantity $hr\sigma_T/P$ are shown; **e** Exemplary truss of 108 members; **f** Truss of 374 members; **g** Change of longitudinal forces (divided by P) in the upper external members of the truss of Fig. 1e

that the lower reinforcing bar DC does not work, which corresponds to the case $\varphi=\pi/10$; we remember that this angle is measured between the RN direction and the force direction, counterclockwise. The whole force is transmitted by the bar RBD: $F_T=P$; in the bar NCD we have $F_C=0$. Position of point P is given by Cartesian coordinates with respect to the (x, y) frame: $x_P=2.738747132r$; $y_P=0.9680382174r$, or by the values $\alpha_p=\frac{2\pi}{5}$; $\beta_p=\frac{\pi}{4}$ characterizing also the angles of the lower and upper fans. Distance of the point P to the supporting line is $d=|x_0(\mathrm{P})|=3.32819983r$. Parameterization of the domains RBA, NAC and ABDC is described in Figs. III.1 and III.2.

By using (III 5.7 and 5.8) we compute the reactions at the upper supporting node R:

$$H_g = \int_0^{\beta_p} T_1^{RBA}(\alpha_1, \beta)\sin\left(\frac{\pi}{4}+\beta\right)d\beta + F_T \sin\left(\frac{\pi}{4}+\beta_p\right) = 2.119128363P$$

$$V_g = \int_0^{\beta_p} T_1^{RBA}(\alpha_1, \beta)\cos\left(\frac{\pi}{4}+\beta\right)d\beta + F_T \cos\left(\frac{\pi}{4}+\beta_p\right) = 0.5035531419P$$

and at the lower supporting node N

$$H_d = \int_0^{\alpha_p} T_2^{NAC}(\alpha, \beta_1)\sin\left(\frac{\pi}{4}+\alpha\right)d\alpha + F_C \sin\left(\frac{\pi}{4}+\alpha_p\right) = -1.810111369P$$

$$V_d = \int_0^{\alpha_p} (-T_2^{NAC}(\alpha, \beta_1))\cos\left(\frac{\pi}{4}+\alpha\right)d\alpha - F_C \cos\left(\frac{\pi}{4}+\alpha_p\right) = 0.4475033745P$$

The reactions H_g, H_d are directed opposite to x_0, and V_g, V_d are directed along y_0.

Notation V_d, V_g should not be misinterpreted as volumes. The non-dimensional volume is defined by $\overline{V} = V/V_0$, $V_0 = Pr/\sigma$. We compute the volumes of the fans NAC, RBA: $\overline{V}_{NAC} = 1.987586823$, $\overline{V}_{RBA} = 1.258902591$. The volume of the Prager–Hill domain ABDC equals $\overline{V}_{ABDC} = 3.565259273$. The total volume of fibres in the fibrous domains is $\overline{V}_S = 6.811748687$. We compute the volumes of the reinforcing bars: the tension bar, $\overline{V}_T = 4.246489413$; and the compression bar, $\overline{V}_C = 0$. The total volume of the reinforcing bars is $\overline{V}_K = 4.246489413$. The total volume of the material of the structure is $\overline{V} = \overline{V}_S + \overline{V}_K = 11.05823810$. The volume of the structure by Michell's formula (I.2.12), $\overline{V} = 11.05823810$, is given by the same number.

The force field T_1 suffers a jump along AC, while the force field T_2 has a jump along the line AB. Both lines AB and AC are the lines of discontinuity of the field h, since along these lines, at least one of the fields A, B, T_1, T_2 suffers a jump. The big values of the function h at the neighbourhood of point A are caused by small values of Lamé coefficients A and B in this domain. Function h grows to infinity at points N and R; one of the Lamé coefficients vanishes there.

The example considered here is specific because the force is applied such that the force in the tension bar is equal to the force applied, while the compression bar does not work. This makes it possible to figure out how the internal force fields T_1 and T_2 satisfy the boundary conditions: the boundary condition along the compression bar reads $T_1 = -F_C$, but here, $T_1 = 0$ (see Fig. 1b). The boundary condition for T_2 along the tension bar assumes the form $T_2 = -F_T$ (see Fig. 1c), showing that the values of T_2 are constant along the tension bar.

The optimal cantilever found becomes a discrete–continuous structure; it can be viewed as a limit of a sequence of trusses of finite number of joints. We show below that the optimal cantilever can indeed be constructed by forming an appropriate sequence of trusses and passing to the limit. To this end we consider the sequence of trusses of joints lying at the selected points of intersection of the parametric lines. The trusses are formed for arbitrary values of the fan angles, for arbitrary number of nodes and for arbitrary (yet admissible) force direction. All the trusses constructed are statically determinate—just as this is the crucial feature of this design sequence, enabling a direct determination of cross sections by the values of the forces in the members and, consequently, enabling for computation of the total volume.

The exemplary truss (Fig. 1e) approximating the Michell cantilever of Fig. 1 possesses 108 members and 56 joints. By assuming that the members are fully stressed we fix the cross sections and compute the volume of the truss as $11.08633976V_0$. Volume of the external bars is $4.780978146V_0$. Volume of the internal bars is $6.305361614V_0$. Volume of the lower (compression) external members is $0.2826225365V_0$. Volume of the upper (tension) external members is $4.498355609V_0$.

The volume of the truss turns out to be bigger than the volume of the Michell structure by about 0.25%. A bigger difference is visible in the division of the volume into the volumes of the external and internal parts. The volume of the internal members of the truss is 92.56% of the volume of the fibrous domain of the optimal cantilever. Moreover, we note that the volume of the external compressed members of the truss is not zero, as in the optimal solution, but is nevertheless much smaller than the volume of the external tension members.

The values of forces in the external members are bigger than a constant value predicted in the optimal solution. The biggest is the force in the member at the support—it is bigger by 10% than the force in the member at node P. The variation of the values of the forces in the external tension members is caused by interaction with internal members which form acute angles (they cannot form right angles in the optimal solution) with external members; the external members can only approximate the trajectory of virtual deformations.

Consider now a truss of larger number of members loaded as before (see Fig. 1f). It has 374 members and 189 joints. Volume of the truss is $11.06524488V_0$. Volume of external members is $4.508915026V_0$. Volume of internal members is $6.556329854V_0$. Volume of external (lower) compression members is $0.1392986978V_0$. Volume of external (upper) tension members is $4.369616328V_0$.

The total volume of the truss differs from the volume of the Michell structure by only 0.063%. The volume of the external members becomes smaller. The volume of the internal members of the truss is now 96.1% of the volume of the Michell structure. The variation of the values of longitudinal forces in the external members is now smaller; the deviation from the exact constant value of the force is now smaller than 5%.

3 Chan-like cantilevers

3.1 The point load at the boundary BH

The cantilever considered is augmented with Chan-like domain. The volume of fibres in this domain is computed by an iterated integral. The force in the upper external bar varies along the boundary, and its volume is computed by appropriate line integration. The analysis of the properties of such an optimal cantilever will be shown by a concrete example (see Fig. 2).

We have here $r_1 = |\mathrm{AN}| = a/2$, $r_2 = |\mathrm{RA}| = a\sqrt{3}/2$, a=|RN|, κ=3. The angle of the upper circular fan is θ_2= $2\pi/9$. Coordinates of the point P are α_p=$7\pi/18$; β_p=$11\pi/18$. Direction of the force is φ=$\pi/5$. The Cartesian coordinates of point P=H, measured in the (x,y) frame are x_P= 1.593994062 a; y_P= 2.064201430 a. Distance of point P to the supporting line RN is d= 3.017660610 a. We can compute the forces in the reinforcing bars at node P=H: F_T (P)=0.8290375726P; F_C(P)=−0.5591929034P

Reactions at the upper supporting node R is H_g =2.383536711P, V_g=1.284829035P
Reactions at the lower supporting node N is H_d= −1.795751459P, V_d=−0.4758120425P

The non-dimensional volume is defined by $\overline{V} = V/\widetilde{V}_0$ with $\widetilde{V}_0 = Pa/\sigma_T$. The volumes of fibres in the fibrous domains are

$$\overline{V}_{NAC} = 2.186540186,\ \overline{V}_{RBA} = 0.9237368385,$$
$$\overline{V}_{ABDC} = 3.750368950,\ \overline{V}_{BDH} = 1.633409910.$$

The total volume of fibres in the fibrous domains is $\overline{V}_S =$ 8.494055884.

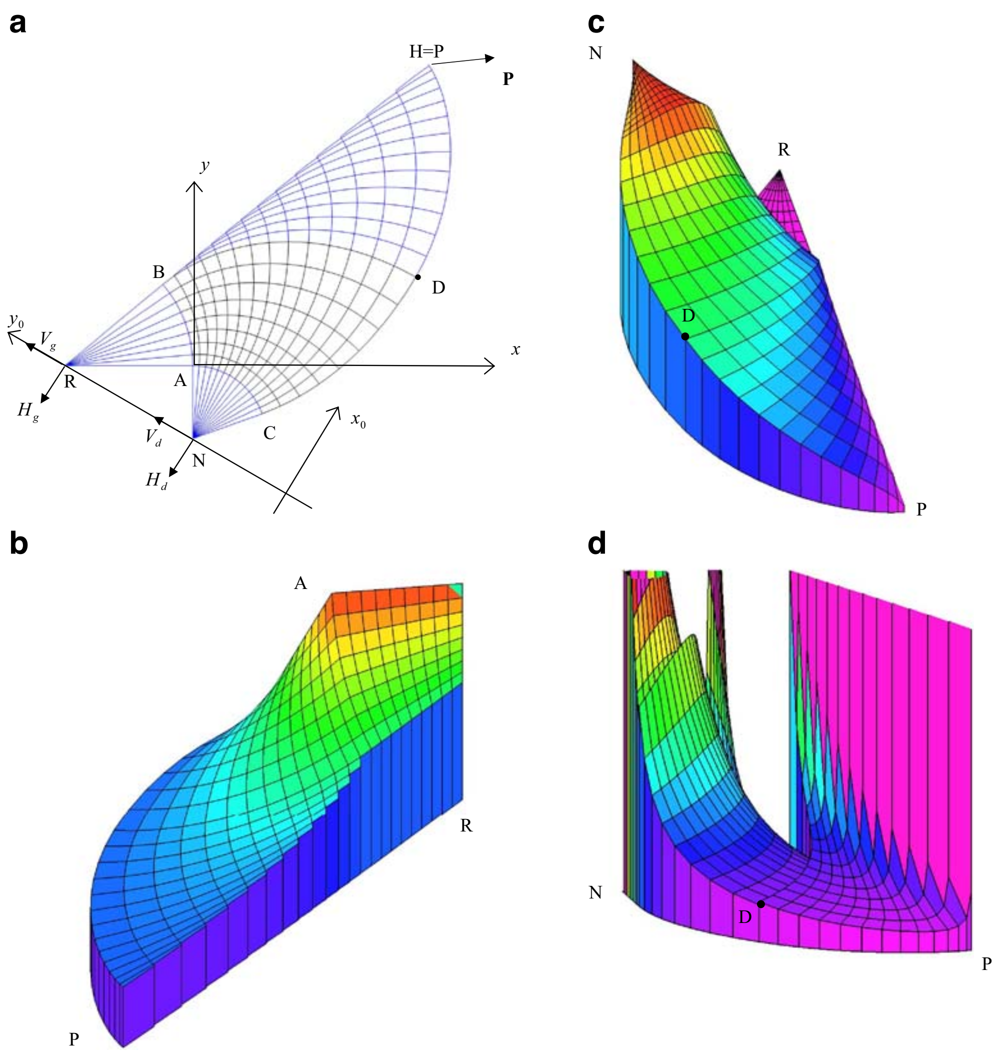

Fig. 2 **a** The cantilever loaded at the line BH. Here, P=H; **b** The force field T_1; **c** The force field T_2; **d** Density of fibres h

We compute the volume of reinforcing bars. Volumes of the tension bar and of the compression bars are $\overline{V}_T = 4.146566250$ and $\overline{V}_C = 5.796540063$, respectively. Total volume of the reinforcing bars is $\overline{V}_K = 9.943106313$. Total volume equals $\overline{V} = \overline{V}_S + \overline{V}_K = 18.43716220$.

The same total volume, but computed by (I.2.12), equals $\overline{V} = 18.43716218$.

The force field T_1 suffers a jump along the line AC or along the boundary between Hill's domain (III) and the circular domain II_d (see Fig. III.4) . This force is continuous along BD, where the Hill domain touches Chan's domain IV. Moreover, the force T_1 is constant along the compression bar. The force field T_2 suffers a jump along AB or along the boundary between Hill's domain (III) and the upper circular domain. The force T_2 is continuous along BD, similarly as T_1 and vanishes along the straight boundary BH.

Every line of the geometric division is a line of discontinuity of the effective density of fibres h because this quantity depends both on Lamé coefficients and force fields. The density of fibres h tends to infinity at points where one of the Lamé coefficients vanishes. This holds at points N and R and along the whole line BH. Indeed, the lines α go to BH tangentially, which means that the area density of these lines around BH must be infinite.

It is worth emphasizing here that this infinitely dense package of fibres along BH is not sufficient to strengthen the boundary. This boundary must be additionally reinforced by a bar of finite cross section.

3.2 The point load applied within domain BDH

To be specific we consider a concrete example, cf. Fig. 3. The entities are the same as in Section 2.

The ratio of allowable stresses is κ=1. We write σ_T= σ_C=σ. The angle of the upper fan is $\theta_2 = \frac{2\pi}{5}$. Curvilinear coordinates of point P are $\alpha_p = \frac{3\pi}{10}$; $\beta_p = \frac{3\pi}{5}$. Angle between the force direction and the supporting line RN is $\varphi = \frac{\pi}{5}$. Cartesian coordinates (x, y) of point P are x_P=0.706548421r; y_P=4.347572630r. Distance between the point P and the supporting line is d=4.2809100497r.

The forces in the reinforcing bars are F_T= 0.4539904998 P and F_C=−0.8910065242 P.

Reaction forces at the upper supporting node R are H_g= 3.812906196 P and V_g=0.1353238651 P.
Reaction forces at the lower supporting node are H_d= −3.225120945 P and V_d=0.6736931261 P.

The non-dimensional volumes are defined as in example 2.1. Volumes of material within the fibrous regions

$$\begin{aligned} \overline{V}_{NMC} &= 0.8003150410, & \overline{V}_{NAM} &= 1.774085275, \\ \overline{V}_{RBA} &= 3.001533208, & \overline{V}_{MQDC} &= 2.835794214, \\ \overline{V}_{ABQM} &= 4.567136096, & \overline{V}_{ZPDQ} &= 1.261828008, \\ \overline{V}_{BZQ} &= 0.8789743173. \end{aligned}$$

The total volume of the material within the fibrous domain is $\overline{V}_S = 15.11966616$.

Volumes of the reinforcing tension and compression bars are $\overline{V}_T = 3.518088666$ and $\overline{V}_C = 5.697963659$, respectively.

The total volume of the reinforcing bars: $\overline{V}_K = 9.216052325$.

The total volume of the material within the whole structure is $\overline{V} = \overline{V}_S + \overline{V}_K = 24.33571848$.

The total volume of the material within the whole structure computed by (I.2.12) is $\overline{V} = 24.33571848$.

The graph of T_1 is similar to the case of the point load being applied at the boundary of Chan's domain IV_g. Along PC the force T_1 is constant and equal (up to the sign) to the longitudinal force in the compression bar. The force T_1 achieves a maximal constant value on the straight segment RA. On the lower circular fan the force T_1 vanishes. Thus, the arc AC is the only discontinuity line for this force field.

The graph of the force T_2 has a specific shape not occurring up till now. Along the segment PZ of the boundary of the region IV (see Fig. III.6), this force assumes the absolute value equal to the longitudinal force in the tension bar. On the other hand, this force vanishes along the segment ZB of the boundary of the Chan-like domain. A discontinuity of this force occurs at point Z, where the natural boundary condition changes its character. This discontinuity extends towards the domains IV, III and II along the line ZQMN. The value of the jump is constant along this line and equals F_T (P); this is just the value of T_2 along ZP. The values of T_2 increase from the boundary of Chan's domain IV_g towards the beginning of the parametric line along which this force is acting. The maximum is achieved on the straight line AN.

Thus, the discontinuity lines of the density function h are

BD, the interface between Hill's domain III and Chan's domain IV_g (there A jumps);
ZN, the interface between the domains of type 1 and 2 (there the force T_2 jumps);
AB, there both A and T_2 suffer jumps; AC, there B and T_1 suffer jumps.

We note that the subdomains of continuity of function h appear as a result of the overlapping of the static and geometric subdivision. This leads to a complicated form of the graph of function h. This function tends to infinity along the straight segment BZ and at the supporting nodes N and R. A highly irregular behaviour of function h is observed around point A.

The analytical results are checked by analysis of trusses of finite number of joints. We consider first a truss of 162 members and 83 nodes, see Fig. 3e. We assume that the members are fully stressed and compute the volume of the material of the truss, 24.39800388V_0, while the volume of the external members is 10.24421848V_0, and the volume of the internal members equals 14.15378540V_0. Volume of the upper external tension members is 3.790527422V_0, and the volume of the lower external compression members equals 6.453691055V_0.

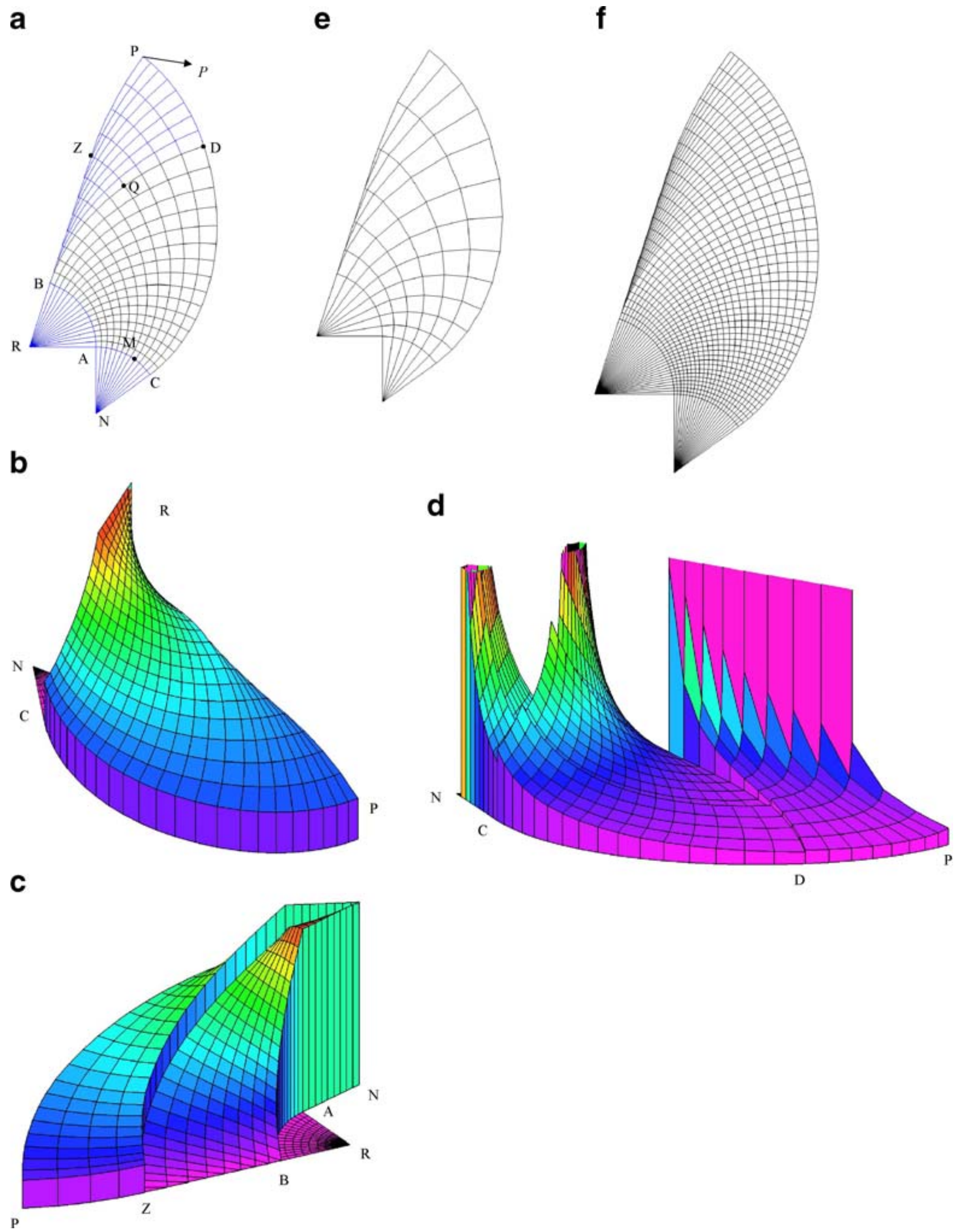

Fig. 3 **a** The cantilever considered. The segment BZ is straight, as lying along the boundary of the feasible domain Ω_0; **b** The force field T_1; **c** The force field T_2; **d** Effective density of the fibres h; **e** A truss with 83 nodes at the intersection points of the Hencky net; **f** The truss of 1091 joints; **g** graph of the force in the upper external bars of the truss of Fig. 3f; **h** graph of the force in the upper reinforcing bar RBZP of the optimal Michell structure; **i** Graph of the force in the lower external members of the truss of Fig. 3f

The volume of the truss is bigger than the volume of the material used for the Michell structure by 0.256%. The internal members contribute to 58.012% of the total volume, whilst for the optimal cantilever, this contribution equals 62.129%.

While analysing variation of the longitudinal force in the upper tension bars, one observes an almost constant value of the force in the first three members counting from point P: in the two members along α line and in the first additional bar. This is because the internal members are almost orthogonally linked with the external ones there. In the four next members the force increases 2,5 times, which is caused by the appearance of the almost tangent members. On the other hand, the change of the force in the external compression members is very small (not bigger than 15%) because no tangent members are present there.

We consider now the truss of a larger number of joints, 1,091 and of 2,178 members, see Fig. 3f. Now, the volume of

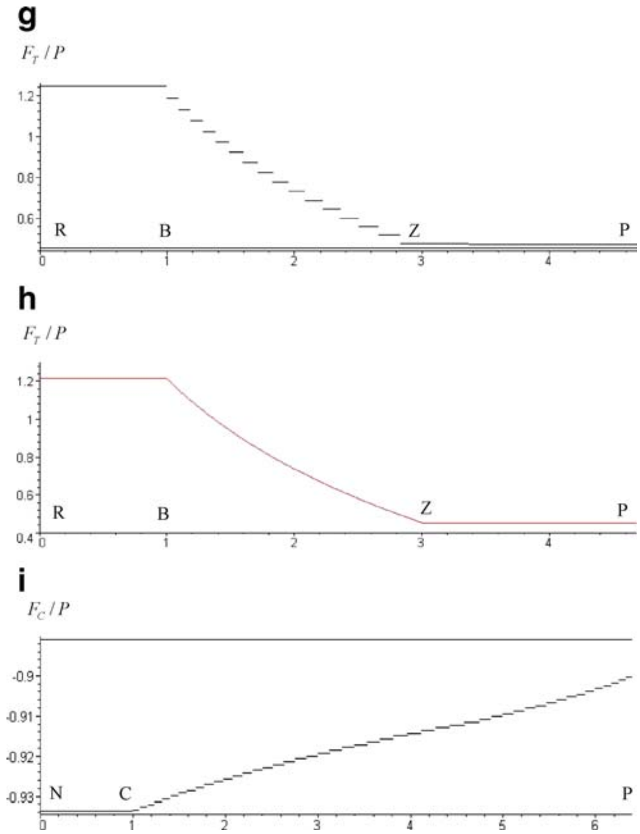

Fig. 3 (Continued)

the material of the truss is $24.33960822V_0$; volume of external members is $9.458673821V_0$; volume of internal members is $14.88093440V_0$. The volume of the upper external tension members is $3.580848790V_0$ and the volume of the lower external tension members is $5.877825031V_0$.

The volume of the material used for constructing the truss of Fig. 3e is almost the same as the volume of the material of the Michell structure; the difference is 0.016%. Contribution of the internal members is greater now (61.139% of the total volume); the contribution of the external members is smaller than in the previous approximation. The force in the tension members is practically constant in the first nine members counting from point P. It then increases, achieving the value 1,243 P at the supporting node R. The analogous value in the Michell structure equals 1,214 P. Thus, the graph 3g shows coincidence with the theoretical prediction in Fig. 3h of the tension force in the upper reinforcing bar. The longitudinal forces in the compression bar are not constant. Their increase is about 3.69%.

4 The cantilevers associated with the force applied within domain DHJG

4.1 Case of κ=1

The geometric division of the feasible domain Ω_0 is shown in Fig. I.19. If the point load P is applied within DHJG, then the optimal cantilever will be included within RBHJGCN. Position of the point load introduces the external boundaries: RBZS_gP and NCZ$'S_d$P (see Fig. 4). The intervals BZ and CZ$'$ are straight. The aim of this section is to analyse the static work of the optimal cantilever by using the results concerning geometry of Hencky nets (section I.8), virtual displacement fields (section II.7) and force fields (section III.8). To be specific we assume concrete data to fix geometry of the feasible domain, the position and direction of the concentrated force of magnitude P:

$$\theta_1 = \theta_2 = \frac{3\pi}{10}, \qquad x_P = 4.346573703r;$$

$$y_P = 3.737498915r, \ \varphi = -\frac{\pi}{10}$$

where $|\mathrm{RN}| = r\sqrt{2}$; coordinates x_P, y_P are referred to the (x, y) system, as in Fig. 1. Then

$$d = 6.423409349r, \alpha_p = \frac{11\pi}{20}, \ \beta_p = \frac{\pi}{2}.$$

By using the methods of section III.8 we compute the forces in the reinforcing bars:

$$F_T = 0.5877852524\,P, F_C = -0.8090169943\,P,$$

the reactions at R are H_g=4.259331967 P and V_g= 0.4880608891 P, and the reaction forces at N are H_d= −4.568348964 P and V_d=0.4629956217 P. These reactions are directed along $(-x_0)$ and y_0. Having the Lamé coefficients (section I.8) and the force fields (section III.8) we know the distribution of the density function h by (1.2). Appropriate integration gives the non-dimensional volumes $\overline{V} = V/V_0$ of the material within the subdomains shown in Fig. 4; here, V_0=Pr/σ; σ=σ_T=σ_C.

$$\begin{aligned}
&\overline{V}_{NAM} = 1.77494717, && \overline{V}_{NMC} = 0.9002697526,\\
&\overline{V}_{RM'A} = 2.163813476, && \overline{V}_{RBM'} = 0.4821436945,\\
&\overline{V}_{AM'WM} = 3.126098073, && \overline{V}_{MWQ'C} = 1.898471189,\\
&\overline{V}_{BQWM'} = 0.7987535187, && \overline{V}_{CQ'Z'} = 1.785009056,\\
&\overline{V}_{BZQ} = 1.221821872, && \overline{V}_{QDQ'W} = 0.5861877908,\\
&\overline{V}_{Q'DS_dZ'} = 0.979949195473, && \overline{V}_{ZS_gDQ} = 1.583623832,\\
&\overline{V}_{DS_gPS_d} = 3.180358924
\end{aligned}$$

Thus, the total volume of the material within the fibrous domains equals $\overline{V}_S = 20.48144755$. Then we compute the volumes of the tension (T) and compression (C) bars

$$\begin{aligned}
\overline{V}_T &= 6.180644310,\\
\overline{V}_C &= 7.831983019,\\
\overline{V}_K &= \overline{V}_T + \overline{V}_C = 14.01262733.
\end{aligned}$$

The volume of the material used for the whole structure is $\overline{V} = \overline{V}_S + \overline{V}_K = 34.49407488$. The same volume can be computed by the alternative formula (I.2.12). Using the re-

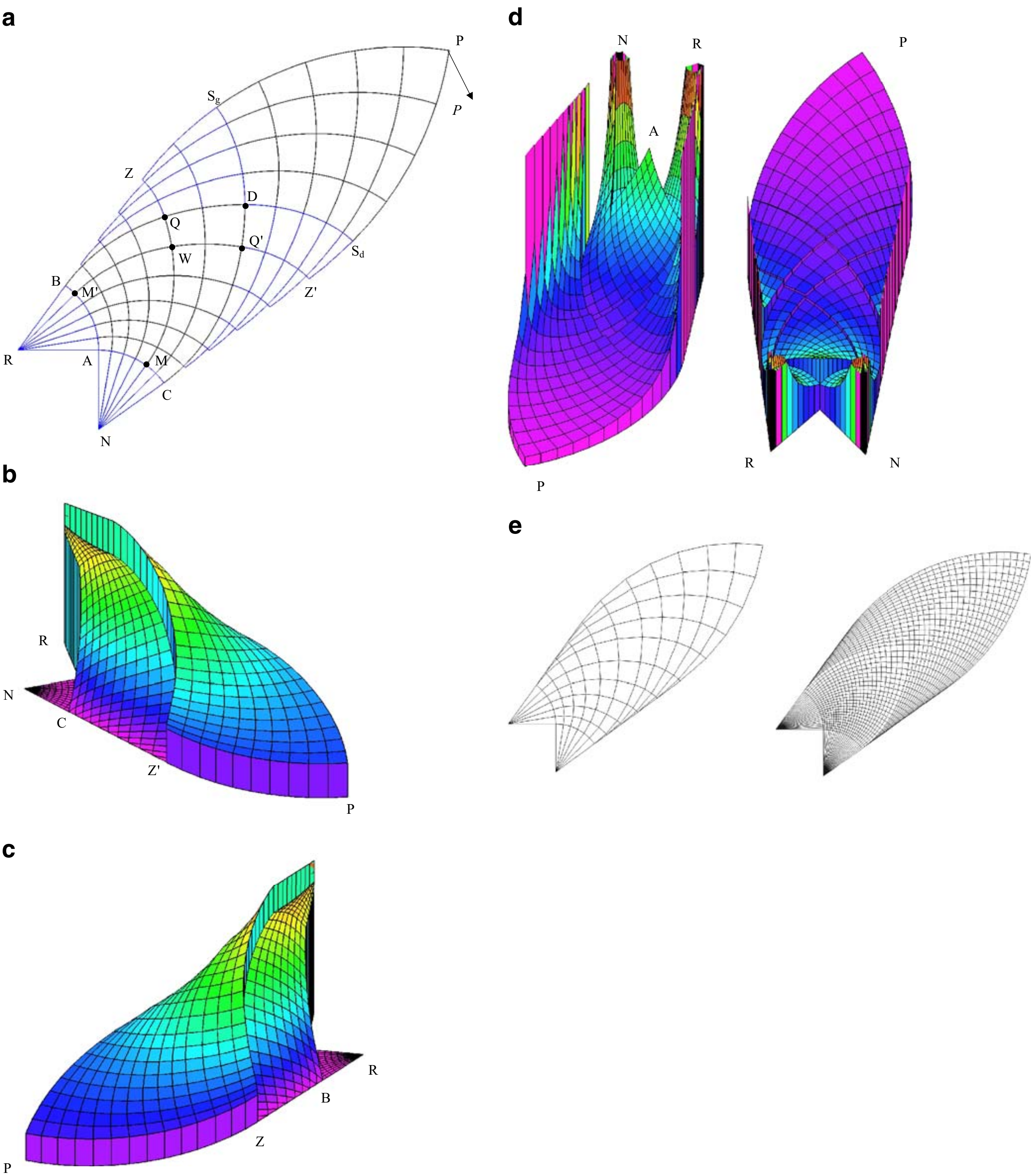

Fig. 4 **a** The cantilever considered. Segments ZR, Z′N lie along the boundaries of the feasible domain Ω_0; **b** Graph of the force field T_1; **c** Graph of the force field T_2; **d** Graph of the density of fibres h; **e** The trusses (1) and (2) of 214 and 2,998 members, respectively. **f** Graph of the longitudinal force in the upper external members of the truss of Fig. 4e (right); **g** Graph of the longitudinal force in the upper reinforcing bar $\mathrm{RBZS_gP}$ of the optimal cantilever; **h** The graph of the force in the lower external members; **i** Graph of the force in the lower external bar of the optimal cantilever

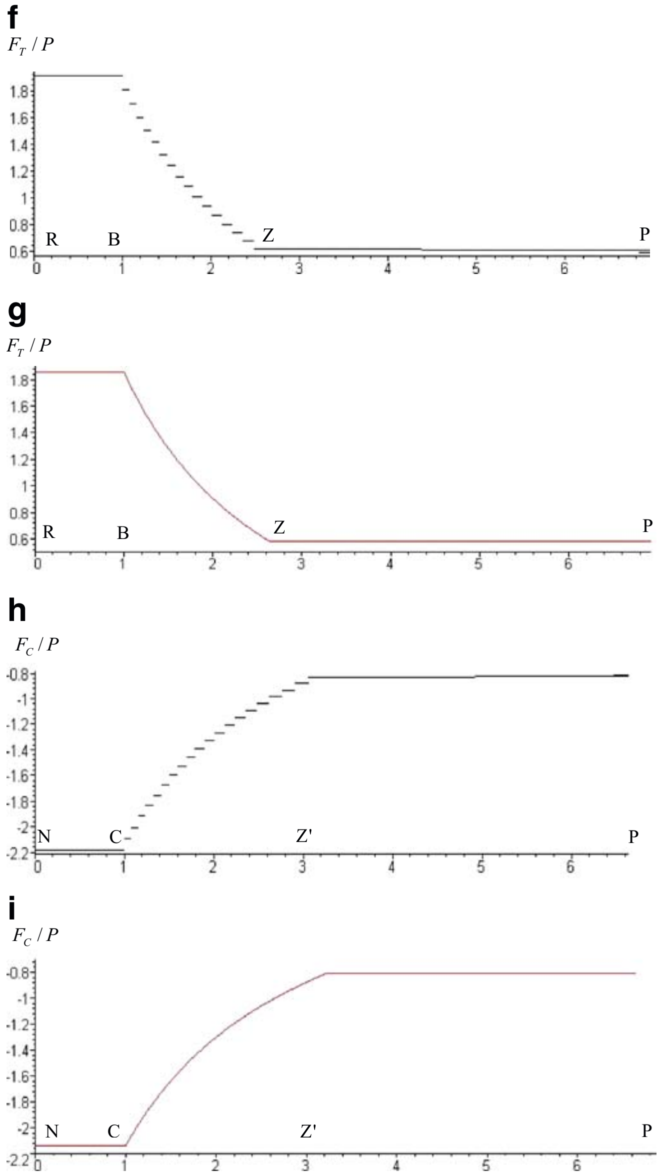

Fig. 4 (Continued)

sults of section II.7 one finds $\overline{V} = 34.49407452$, which confirms the previous result based on the force field analysis.

Distribution of the force field T_1 is seemingly similar to that of example 7, where the point load is applied within Chan's domain IV_d. Then the main part of the cantilever was divided into two subdomains of the static division. The situation now is more complicated. The main part of the cantilever (without circular fans) is divided into four subdomains of the static division, separated by the lines MZ and M′Z′ (see Fig. III.9). In each subdomain the force field T_1 is determined by different formulae. Along the line Z′Q′WM′R we note the jump of T_1 equal to F_C(P). Along MWQZ the force T_1 is continuous; that is why this line is not visible in the graph in Fig. 4b. The graph of T_2 is similar to that of the example in sec. 3.2, where the point load was applied within Chan's domain IV_g. Now the jump of value F_T(P) occurs along MZ, while along M′Z′, the internal force T_2 is continuous.

The graph of the density of fibres function h is constructed by overlapping the graphs of Lamé coefficients and the internal forces T_1 and T_2. Six discontinuity lines appear: two discontinuity lines of the force fields ZN and Z′R, the lines of geometric division $\mathrm{CS_g}$ and $\mathrm{BS_d}$, and the circular arcs AC and AB.

Let us note that all these lines appeared already in the examples in which the point P lay within Chan's domains (upper and lower); these domains are now extended. Thus, the optimal cantilever considered is composed of 13 subdomains in which density h is appropriately determined, the internal boundaries being the discontinuity lines of h. Four subdomains of the final division appear on the two circular domains, four on the Hill's domain, two of them lie on Chan's upper domain and two on Chan's lower domain; one subdomain appears in domain V (see Fig. III.9). Thus, the density function graph is fairly complicated (see Fig. 4d).

The results presented above will be verified by considering two trusses (1,2) of finite number of joints fixed at the selected intersection points of the Hencky net of our problem. The truss (1) of 214 and truss (2) of 2,998 members are shown in Fig. 4e. One can prove that both these trusses are statically determinate. This property makes it easy to fix the cross sections to saturate the stress level. The results of computations are set up in Table 1, where $\overline{V}_S$ for trusses represents the total volume of internal members.

Let us analyse distribution of the longitudinal forces in the external members and compare them with distribution of the forces F_C and F_T in the reinforcing ribs of the Michell structure (see Fig. 4f–i). The nonlinear behaviour of F_T along BZ and of F_C along CZ′ is approximated stepwise (see Fig. 4f, h). Let us note that truss (2) is heavier than the optimal cantilever by 0.015%.

The volume of the truss is bigger than the volume of the material used for Michell-like cantilever by 0.244%. Consider now the volumes of the external and internal members. The latter members occupy 56.125% of the total volume; let us remind that this contribution is 59.376% in the optimal cantilever. Thus, we note a discrepancy much larger than that concerning approximation of the total volume.

The force in the tension-reinforcing bar is constant in the first eight members, then it increases up to the value 2,094 P. This increase is brought about by tangent members going from within the interior. A similar phenomenon is observed

Table 1 Truss approximation results

	Truss 1	Truss 2	Michell structure
Number of members	214	2,998	Infinite
Number of joints	109	1,501	Infinite
$\overline{V}$	34.57834674	34.49933802	34.49407
$\overline{V}_T$	6.851381387	6.336352716	6.1806443
$\overline{V}_C$	8.319861742	7.94368072	7.831983
$\overline{V}_K$	15.17124313	14.28003344	14.012627
$\overline{V}_S$	19.40710361	20.21930458	20.481447

in the external line of compression members: the force is constant in the first six members, and then its absolute value increases and achieves the maximal value 2,345 P at the supporting node.

The truss is heavier than the optimal cantilever by 0.015%. The internal members contribute to 58.61% of the total volume. The longitudinal force in the upper external tension members varies from 0.604P to 1,911P, while the force in the compression external members varies from $-0{,}821P$ to $-2{,}189P$. The corresponding values of the optimal cantilever are from 0,587P to 1,856P and from $-0{,}809P$ to $-2{,}141P$. The graphs of the force distribution in the external members compare favorably with their counterparts in the optimal cantilever.

4.2 Case of κ=3

To be specific we assume concrete data, see Fig. 5a

$$\theta_1 = \frac{\pi}{6}; \qquad \theta_2 = \frac{5\pi}{12},\ x_P = 1.557879337\ a;$$
$$y_P = 2.994292715\ a,\ \varphi = \frac{\pi}{8},$$

where a=|RN|; coordinates x_P, y_P are referred to the (x,y) system (as in Fig. 1). Then

$$d = 3.805085930\,a,\ \alpha_p = \frac{\pi}{2},\ \beta_p = \frac{\pi}{2}.$$

By using the methods of section III.8 we compute the forces in the reinforcing bars:

$$F_T = 0.6087614290\ P;\ F_C = -0.7933533403\ P$$

and compute the reactions at R as H_g=3.363139403 P, V_g= 0.5613526265 P and the reaction forces at N as H_d= -3.74582283 P, V_d=0.3625269006 P. These reactions are directed along ($-x_0$) and y_0. Having the Lamé coefficients (section I.8) and the force fields (section III.8), we know the distribution of the density function h by (1.2). Appropriate integration gives the non-dimensional volumes $\overline{V} = V/\widetilde{V}_0$ of the material within the subdomains shown in Fig. 5a; here, $\widetilde{V}_0 = Pa/\sigma_T$;

$$\begin{aligned}
\overline{V}_{NAM} &= 1.03291971, & \overline{V}_{NMC} &= 1.095218421,\\
\overline{V}_{RM'A} &= 1.738224285, & \overline{V}_{RBM'} &= 0\ .5492020058,\\
\overline{V}_{AM'WM} &= 1.957767017, & \overline{V}_{MWQ'C} &= 2.749061275,\\
\overline{V}_{BQWM'} &= 0.3951255746, & \overline{V}_{CQ'Z'} &= 4.825841085,\\
\overline{V}_{BZQ} &= 0.1280375442, & \overline{V}_{QDQ'W} &= 0.7147046372,\\
\overline{V}_{Q'DS_dZ'} &= 2.807816353, & \overline{V}_{ZS_gDQ} &= 0.3647799660,\\
\overline{V}_{DS_gPS_d} &= 1.823721477. & &
\end{aligned}$$

Thus, the total volume of the material within the fibrous domains equals $\overline{V}_S = 20.18241935$. Then we compute the volumes of the tension (T) and compression (C) bars

$$\begin{aligned}
\overline{V}_T &= 3.086166189,\\
\overline{V}_C &= 14.67228125,\\
\overline{V}_K &= \overline{V}_T + \overline{V}_C = 17.75844744.
\end{aligned}$$

The volume of the material used for the whole structure is $\overline{V} = \overline{V}_S + \overline{V}_K = 37.94086679$. The same volume can be computed by the alternative formula (I.2.12). Using the results of section II.7 one finds $\overline{V} = 37.94086663$, which confirms the previous result based on the force field analysis.

We note that T_2=const along PZ, then it vanishes along ZBR (see Fig. 5b). Along ZM this force field jumps. Its maximum is attained along NC.

5 The case of the concentrated force applied at a point within $JH_2J_2G_2$

Now we consider a longer cantilever, transmitting the point load applied within $JH_2J_2G_2$ to the supporting line RN. We assume that σ=σ_T=σ_C (or κ=1) and θ_1=θ_2=θ=3π/10. The key to the solution of the equilibrium problem of Fig. 6 is to figure out the division of the cantilever domain, which is a result of an overlapping of the kinematic division explained in Fig. I.19, denoted by Roman numerals (I,II,...,VII), and of the static division of Fig. III.11, denoted by Arabic numbers (1,2,...,7), as superscripts. The indices g and d mean the upper or lower domain, respectively. This example is fairly complicated, but since it could serve as a benchmark, the indispensable details will nevertheless be reported.

Thus, the domain of the cantilever is divided into the following 23 subdomains:

$$\begin{aligned}
&\mathrm{RAM'} = \mathrm{II}^7_g, && \mathrm{NAM} = \mathrm{II}^7_d,\\
&\mathrm{AM'}WM = \mathrm{III}^7, && \mathrm{RBM'} = \mathrm{II}^6_g,\\
&\mathrm{BM'WQ} = \mathrm{III}^6, && \mathrm{BQZ} = \mathrm{IV}^6_g,\\
&\mathrm{NMC} = \mathrm{II}^5_d, && \mathrm{CMWQ'} = \mathrm{III}^5,\\
&\mathrm{CQ'Z'} = \mathrm{IV}^5_d, && \mathrm{WQDQ'} = \mathrm{III}^4,\\
&\mathrm{Q'DZ'_1Z'} = \mathrm{IV}^4_d, && \mathrm{QZZ_1D} = \mathrm{IV}^4_g,\\
&\mathrm{DZ_1W_1Z'} = \mathrm{V}^4, && \mathrm{Z'Z'_1G} = \mathrm{IV}^3_d,\\
&\mathrm{GZ'_1W_1Z_d} = \mathrm{V}^3, && \mathrm{GQ'_1Z_d} = \mathrm{VI}^3_d,\\
&\mathrm{ZZ_1H} = \mathrm{IV}^2_g, && \mathrm{Z_1W_1Q_1H} = \mathrm{V}^2,\\
&\mathrm{HQ_1Z_g} = \mathrm{VI}^2_g, && \mathrm{W_1Q_1D_1Q'_1} = \mathrm{V}^1,\\
&\mathrm{Q'_1D_1H_1Z_d} = \mathrm{VI}^1_d, && \mathrm{Q_1D_1G_1Z_g} = \mathrm{VI}^1_g,\\
&\mathrm{D_1G_1PH_1} = \mathrm{VII}^1. &&
\end{aligned}$$

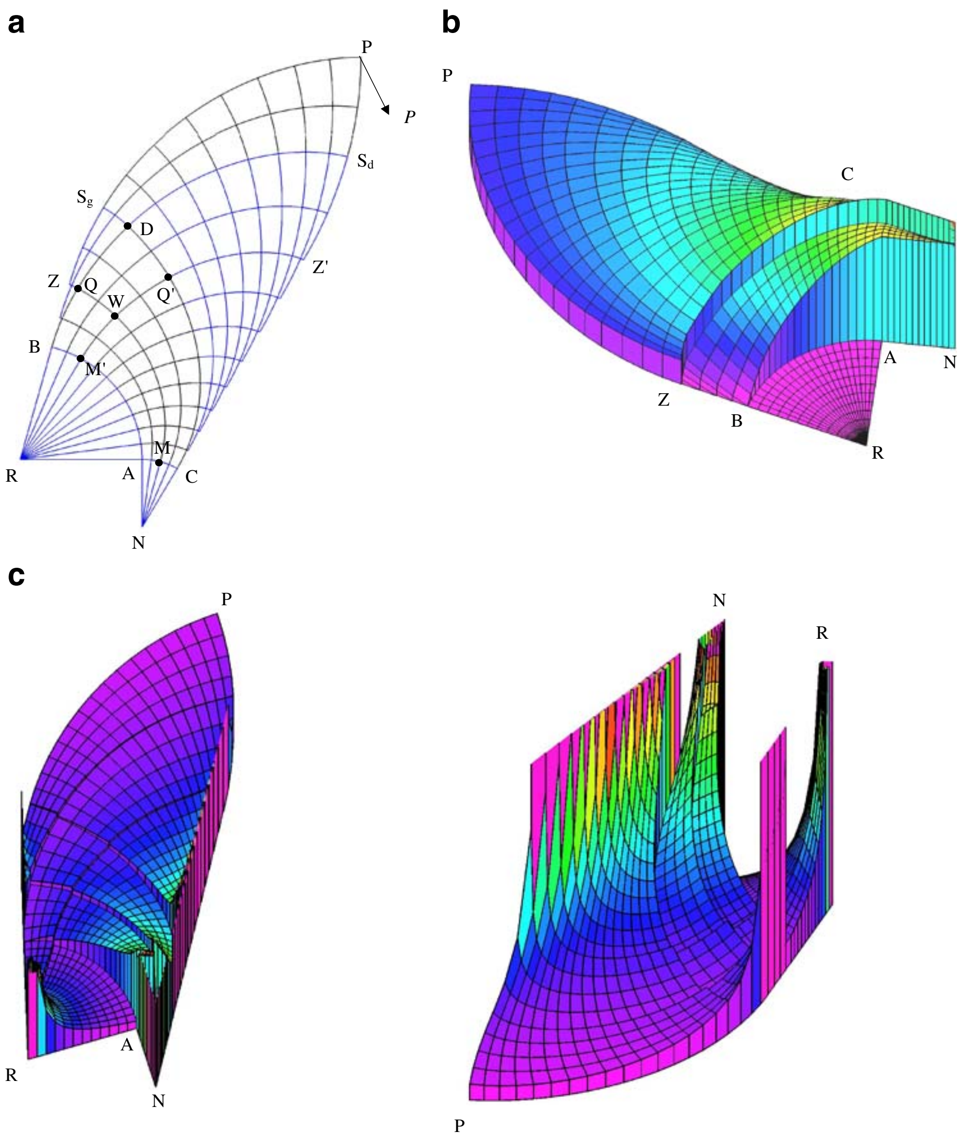

Fig. 5 **a** The cantilever considered; **b** Graph of the force field T_2; **c** Graph of the density of fibres function h

The vertices of these domains have the following curvilinear coordinates (α, β):

$$
\begin{array}{llll}
\mathrm{P} & = (\alpha_p, \beta_p), & \mathrm{B} & = (0, \theta), \\
\mathrm{M}' & = (0, \beta_p - 2\theta), & \mathrm{A} & = (0, 0), \\
\mathrm{M} & = (\alpha_p - 2\theta, 0), & \mathrm{C} & = (\theta, 0), \\
\mathrm{W} & = (\alpha_p - 2\theta, \beta_p - 2\theta), & \mathrm{Q}' & = (\theta, \beta_p - 2\theta), \\
\mathrm{Q} & = (\alpha_p - 2\theta, \theta), & \mathrm{D} & = (\theta, \theta), \\
\mathrm{Z} & = (\alpha_p - 2\theta, \alpha_p - \theta), & \mathrm{Z}' & = (\beta_p - \theta, \beta_p - 2\theta), \\
\mathrm{G} & = (2\theta, \theta), & \mathrm{Z}'_1 & = (\beta_p - \theta, \theta), \\
\mathrm{Z}_1 & = (\theta, \alpha_p - \theta), & \mathrm{H} & = (\theta, 2\theta), \\
W_1 & = (\beta_p - \theta, \alpha_p - \theta), & \mathrm{Q}_1 & = (\beta_p - \theta, 2\theta), \\
\mathrm{Q}'_1 & = (2\theta, \alpha_p - \theta), & \mathrm{D}_1 & = (2\theta, 2\theta),
\end{array}
$$

$$
\mathrm{Z_g} = (\beta_p - \theta, \beta_p),\ \mathrm{Z_d} = (\alpha_p, \alpha_p - \theta),
$$
$$
\mathrm{G}_1 = (2\theta, \beta_p), \qquad \mathrm{H}_1 = (\alpha_p, 2\theta).
$$

We shall report the results corresponding to the following data:

$$
\alpha_p = \frac{17\pi}{20};\ \beta_p = \frac{4\pi}{5};\ \varphi = \frac{\pi}{10};\ d = 13.01824557r.
$$

Not all the details of the analysis will be given. The results below follow from numerous formulae reported in the previous parts of the paper. We start with Cartesian coordinates [referred to (x,y) frame of Fig. 1] of point P: x_P=9.188744886r; y_P=8.221834561r. We compute the

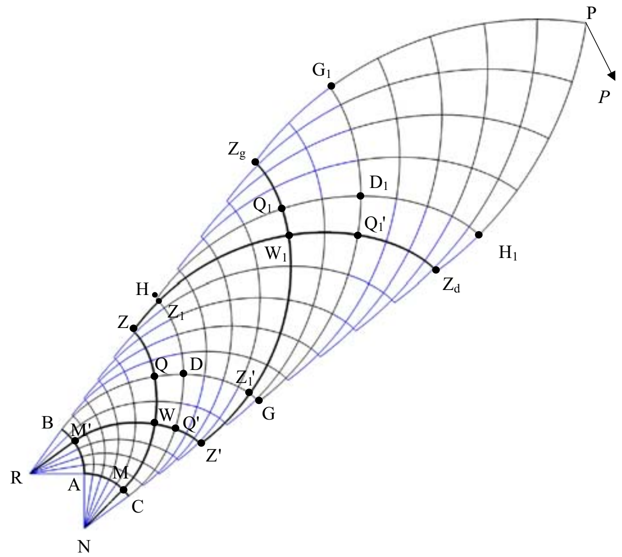

Fig. 6 Subdivision of the optimal cantilever into the domains of static and geometric divisions. Case of point P lying within the domain VII

forces in the reinforcing bars at node P as F_T(P)= 0.9510565165 P; F_C(P)=−0.3090169938 P. Reaction forces at the upper supporting node are computed as follows:

$$H_g = \int_0^{\beta_p-2\theta} T_1^{IIg7}(1,\beta)\sin\left(\frac{\pi}{4}+\beta\right)d\beta + \int_{\beta_p-2\theta}^{\theta} T_1^{IIg6}(1,\beta)\sin\left(\frac{\pi}{4}+\beta\right)d\beta + F_T(\mathrm{B})\sin\left(\frac{\pi}{4}+\theta\right),$$

where F_T (B) is given by (III.9.17b) for α=0; $T_1{}^{IIg7}$ (or $T_1{}^{IIg6}$) means T_1 within domain II_g^7 (or II_g^6);

$$V_g = \int_0^{\beta_p-2\theta} T_1^{III7}(1,\beta)\cos\left(\frac{\pi}{4}+\beta\right)d\beta + \int_{\beta_p-2\theta}^{\theta} T_1^{\mathrm{III}5}(1,\beta)\cos\left(\frac{\pi}{4}+\beta\right)d\beta + F_T(\mathrm{B})\cos\left(\frac{\pi}{4}+\theta\right),$$

which gives H_g=8.759863521 P and V_g=0.4486582529 P. Reaction forces at the lower supporting node are computed as follows:

$$H_d = \int_0^{\alpha_p-2\theta} T_2^{IId7}(\alpha,1)\sin\left(\frac{\pi}{4}+\alpha\right)d\alpha + \int_{\alpha_p-2\theta}^{\theta} T_2^{IId5}(\alpha,1)\sin\left(\frac{\pi}{4}+\alpha\right)d\alpha + F_C(\mathrm{C})\sin\left(\frac{\pi}{4}+\theta\right),$$

where F_C(C) is given by (III.9.18b) for β=0;

$$V_d = -\int_0^{\alpha_p-2\theta} T_2^{IId7}(\alpha,1)\cos\left(\frac{\pi}{4}+\alpha\right)d\alpha - \int_{\alpha_p-2\theta}^{\theta} T_2^{IId5}(\alpha,1)\cos\left(\frac{\pi}{4}+\alpha\right)d\alpha - F_C(\mathrm{C})\cos\left(\frac{\pi}{4}+\theta\right),$$

which gives H_d=−8.450846479 P and V_d=0.5023981407 P.

The volumes of the material within the fibrous domains are denoted according to the notation of Fig. III.11 and Fig. 6. To make the analysis complete we shall put forward all the formulae for the volumes of the subdomains into which the structure is divided.

The volume of the lower circular internal fan NAM (see Fig. 6) is

$$V^{IId7} = \int_0^1 \int_0^{\alpha_p-2\theta} A^{IId7}(\alpha,\beta_1)B^{IId7}(\alpha,\beta_1)h^{IId7}(\alpha,\beta_1)d\alpha d\beta_1;$$

$$V^{IId7} = 3.475700031 V_0,$$

where $V_0 = Pr/\sigma$. The volume of the lower circular external fan NMC is

$$V^{IId5} = \int_0^1 \int_{\alpha_p-2\theta}^{\theta} A^{IId5}(\alpha,\beta_1)B^{IId5}(\alpha,\beta_1)h^{IId5}(\alpha,\beta_1)d\alpha d\beta_1;$$

$$V^{IId5} = 0.6455328237 V_0.$$

The volume of the upper circular internal fan RAM′ is

$$V^{IIg7} = \int_0^{\beta_p-2\theta} \int_0^1 A^{IIg7}(\alpha_1,\beta)B^{IIg7}(\alpha_1,\beta)h^{IIg7}(\alpha_1,\beta)d\alpha_1 d\beta;$$

$$V^{IIg7} = 2.780971414 V_0.$$

The volume of the upper circular external fan RBM′ is

$$V^{IIg6} = \int_{\beta_p-2\theta}^{\theta} \int_0^1 A^{IIg6}(\alpha_1,\beta)B^{IIg6}(\alpha_1,\beta)h^{IIg6}(\alpha_1,\beta)d\alpha_1 d\beta;$$

$$V^{IIg6} = 1.345820099 V_0.$$

The volume of Hill's region AM′WM of the static division 7 is

$$V^{III7} = \int_0^{\beta_p-2\theta} \int_0^{\alpha_p-2\theta} A^{III7}(\alpha,\beta)B^{III7}(\alpha,\beta)h^{III7}(\alpha,\beta)d\alpha d\beta;$$

$$V^{III7} = 4.997932218 V_0.$$

The volume of Hill's region BM′WQ of the static division 6 is

$$V^{III6} = \int_{\beta_p-2\theta}^{\theta} \int_{0}^{\alpha_p-2\theta} A^{III6}(\alpha,\beta) B^{III6}(\alpha,\beta) h^{III6}(\alpha,\beta) d\alpha d\beta;$$
$$V^{III6} = 2.944450720 V_0.$$

The volume of Hill's region CMWQ′ of the static division 5 is

$$V^{III5} = \int_{0}^{\beta_p-2\theta} \int_{\alpha_p-2\theta}^{\theta} A^{III5}(\alpha,\beta) B^{III5}(\alpha,\beta) h^{III5}(\alpha,\beta) d\alpha d\beta;$$
$$V^{III5} = 1.094712407 V_0.$$

The volume of Hill's region WQDQ′ of the static division 4 is

$$V^{III4} = \int_{\beta_p-2\theta}^{\theta} \int_{\alpha_p-2\theta}^{\theta} A^{III4}(\alpha,\beta) B^{III4}(\alpha,\beta) h^{III4}(\alpha,\beta) d\alpha d\beta;$$
$$V^{III4} = 0.7912442817 V_0.$$

The volume of Chan's lower domain CQ′Z′ of the static division 5 is

$$V^{IVd5} = \int_{0}^{\beta_p-2\theta} \int_{\theta}^{\theta+\beta} A^{IVd5}(\alpha,\beta) B^{IVd5}(\alpha,\beta) h^{IVd5}(\alpha,\beta) d\alpha d\beta;$$
$$V^{IVd5} = 1.949485842 V_0.$$

The volume of Chan's lower domain Q′DZ′$_1$Z′ of the static division 4 is

$$V^{IVd4} = \int_{\beta_p-2\theta}^{\theta} \int_{\theta}^{\beta_p+\theta} A^{IVd4}(\alpha,\beta) B^{IVd4}(\alpha,\beta) h^{IVd4}(\alpha,\beta) d\alpha d\beta;$$
$$V^{IVd4} = 2.613805605 V_0.$$

The volume of Chan's lower domain Z′Z′$_1$G of the static division 3 is

$$V^{IVd3} = \int_{\beta_p-2\theta}^{\theta} \int_{\beta_p-\theta}^{\theta+\beta} A^{IVd3}(\alpha,\beta) B^{IVd3}(\alpha,\beta) h^{IVd3}(\alpha,\beta) d\alpha d\beta;$$
$$V^{IVd3} = 0.7153223805 V_0.$$

The volume of Chan's upper domain BQZ of the static division 6 is

$$V^{IVg6} = \int_{0}^{\alpha_p-2\theta} \int_{\theta}^{\theta+\alpha} A^{IVg6}(\alpha,\beta) B^{IVg6}(\alpha,\beta) h^{IVg6}(\alpha,\beta) d\alpha d\beta;$$
$$V^{IVg6} = 3.345627065 V_0.$$

The volume of Chan's upper domain QZZ$_1$D of the static division 4 is

$$V^{IVg4} = \int_{\alpha_p-2\theta}^{\theta} \int_{\theta}^{\alpha_p-\theta} A^{IVg4}(\alpha,\beta) B^{IVg4}(\alpha,\beta) h^{IVg4}(\alpha,\beta) d\alpha d\beta;$$
$$V^{IVg4} = 1.715672751 V_0.$$

The volume of Chan's upper domain ZZ$_1$H of the static division 2 is

$$V^{IVg2} = \int_{\alpha_p-2\theta}^{\theta} \int_{\alpha_p-\theta}^{\theta+\alpha} A^{IVg2}(\alpha,\beta) B^{IVg2}(\alpha,\beta) h^{IVg2}(\alpha,\beta) d\alpha d\beta;$$
$$V^{IVg2} = 0.1564714358 V_0.$$

The volume of the domain V of the static division 4 or DZ$_1$W$_1$Z′ is

$$V^{V4} = \int_{\theta}^{\alpha_p-\theta} \int_{\theta}^{\beta-\theta} A^{V4}(\alpha,\beta) B^{V4}(\alpha,\beta) h^{V4}(\alpha,\beta) d\alpha d\beta;$$
$$V^{V4} = 6.338378990 V_0.$$

The volume of the domain V of the static division 3 or GZ′$_1$W$_1$Z$_d$ is

$$V^{V3} = \int_{\theta}^{\alpha_p-\theta} \int_{\beta_p-\theta}^{2\theta} A^{V3}(\alpha,\beta) B^{V3}(\alpha,\beta) h^{V3}(\alpha,\beta) d\alpha d\beta;$$
$$V^{V3} = 3.543679041 V_0.$$

The volume of the domain V of the static division 2 or Z$_1$W$_1$Q$_1$H is

$$V^{V2} = \int_{\alpha_p-\theta}^{2\theta} \int_{\theta}^{\beta_p-\theta} A^{V2}(\alpha,\beta) B^{V2}(\alpha,\beta) h^{V2}(\alpha,\beta) d\alpha d\beta;$$
$$V^{V2} = 1.213272591 V_0.$$

The volume of the domain V of the static division 1 or W$_1$Q$_1$D$_1$Q′$_1$ is

$$V^{V1} = \int_{\alpha_p-\theta}^{2\theta} \int_{\beta_p-\theta}^{2\theta} A^{V1}(\alpha,\beta) B^{V1}(\alpha,\beta) h^{V1}(\alpha,\beta) d\alpha d\beta;$$
$$V^{V1} = 0.7663860998 V_0.$$

The volume of the second lower Chan's domain GQ′$_1$Z$_d$ of the static division 3 is

$$V^{VId3} = \int_{\theta}^{\alpha_p-\theta} \int_{2\theta}^{\theta+\beta} A^{VId3}(\alpha,\beta) B^{VId3}(\alpha,\beta) h^{VId3}(\alpha,\beta) d\alpha d\beta;$$
$$V^{VId3} = 3.211119411 V_0.$$

The volume of the second lower Chan's domain $Q_1'D_1H_1Z_d$ of the static division 1 is

$$V^{VId1} = \int_{\alpha_p-\theta}^{2\theta}\int_{2\theta}^{\alpha_p} A^{VId1}(\alpha,\beta)B^{VId1}(\alpha,\beta)h^{VId1}(\alpha,\beta)d\alpha d\beta;$$

$V^{VId1} = 1.350077647V_0$.

The volume of the second upper Chan's domain HQ_1Z_g of the static division 2 is

$$V^{VIg2} = \int_{\theta}^{\beta_p-\theta}\int_{2\theta}^{\theta+\alpha} A^{VIg2}(\alpha,\beta)B^{VIg2}(\alpha,\beta)h^{VIg2}(\alpha,\beta)d\alpha d\beta;$$

$V^{VIg2} = 1.969535422V_0$.

The volume of the second upper Chan's domain $Q_1D_1G_1Z_g$ of the static division 1 is

$$V^{VIg1} = \int_{\beta_p-\theta}^{2\theta}\int_{2\theta}^{\beta_p} A^{VIg1}(\alpha,\beta)B^{VIg1}(\alpha,\beta)h^{VIg1}(\alpha,\beta)d\alpha d\beta;$$

$V^{VIg1} = 2.286771699V_0$.

The volume of the domain VII of the static division 1, or $D_1G_1PH_1$ is

$$V^{VII1} = \int_{2\theta}^{\beta_p}\int_{2\theta}^{\alpha_p} A^{VII1}(\alpha,\beta)B^{VII1}(\alpha,\beta)h^{VII1}(\alpha,\beta)d\alpha d\beta;$$

$V^{VII1} = 4.911550402V_0$.

The total volume of the material used for the fibrous domains equals V_S=54.16352037V_0.

We compute the volumes of the reinforcing bars. The tension-reinforcing bar along the domain RBM′ is $V_k^{IIg6} = \sigma^{-1}\cdot F_T^6(\mathrm{B})\cdot r$; V_k^{II6}=5.039527441V_0. The volume of the tension-reinforcing bar along the domain BQZ is

$$V_k^{\mathrm{IVg6}} = \sigma^{-1}\int_0^{\alpha_p-2\theta} A^{IVg6}(\alpha,\alpha+\theta)F_T^6 d\alpha;$$

$V_k^{\mathrm{IVg6}} = 7.772438081V_0$.

The volume of the tension -reinforcing bar along the domain ZZ_1H is

$$V_k^{\mathrm{IVg2}} = \sigma^{-1}\int_{\alpha_p-2\theta}^{\theta} A^{IVg2}(\alpha,\alpha+\theta)F_T^2 d\alpha;$$

$V_k^{\mathrm{IVg2}} = 1.629394719V_0$.

The volume of the tension-reinforcing bar along the domain HQ_1Z_g is

$$V_k^{\mathrm{VIg2}} = \sigma^{-1}\int_{\theta}^{\beta_p-\theta} A^{VIg2}(\alpha,\alpha+\theta)F_T^2 d\alpha;$$

$V_k^{\mathrm{VIg2}} = 4.37933693V_0$.

The volume of the tension-reinforcing bar along the domain $Q_1D_1G_1Z_g$ is

$$V_k^{\mathrm{VIg1}} = \sigma^{-1}\int_{\beta_p-\theta}^{2\theta} A^{VIg1}\big(\alpha,\beta_p\big)F_T d\alpha;$$

$V_k^{\mathrm{VIg1}} = 1.853498369V_0$.

The volume of the tension-reinforcing bar along the domain $D_1G_1PH_1$ is

$$V_k^{\mathrm{VII1}} = \sigma^{-1}\int_{2\theta}^{\alpha_p} A^{VII1}\big(\alpha,\beta_p\big)F_T d\alpha;$$

$V_k^{\mathrm{VII1}} = 4.714622429V_0$.

The total volume of the tension-reinforcing bar is V_T= 5.38881797V_0.

The volume of the reinforcing compression bar along the domain NMC is

$$V_k^{\mathrm{IId5}} = -\sigma^{-1}\cdot F_C^5(\mathrm{C})\cdot r;\ V_k^{\mathrm{IId5}} = 4.733490212V_0.$$

The volume of the reinforcing compression bar along the domain CQ′Z′ is

$$V_k^{\mathrm{IVd5}} = -\sigma^{-1}\int_0^{\beta_p-2\theta} B^{IVd5}(\beta+\theta,\beta)F_C^5 d\beta;$$

$V_k^{\mathrm{IVd5}} = 5.711466545V_0$.

The volume of the reinforcing compression bar along the domain $Z'Z_1'G$ is

$$V_k^{\mathrm{IVd3}} = -\sigma^{-1}\int_{\beta_p-2\theta}^{\theta} B^{IVd3}(\beta+\theta,\beta)F_C^3 d\beta;$$

$V_k^{\mathrm{IVd3}} = 2.753625735V_0$.

The volume of the reinforcing compression bar along the domain $GQ_1'Z_d$ is

$$V_k^{\mathrm{VId3}} = -\sigma^{-1}\int_{\theta}^{\alpha_p-2\theta} B^{VId3}(\beta+\theta,\beta)F_C^3 d\beta;$$

$V_k^{\mathrm{VId3}} = 3.43389751V_0$.

The volume of the reinforcing compression bar along the domain $Q_1'D_1H_1Z_d$ is

$$V_k^{\mathrm{VId1}} = -\sigma^{-1}\int_{\alpha_p-\theta}^{2\theta} B^{VId1}\big(\alpha_p,\beta\big)F_C d\beta;$$

$V_k^{\mathrm{VId1}} = .3160621721V_0$.

The volume of the reinforcing compression bar along the domain $D_1G_1PH_1$ is

$$V_k^{\mathrm{VIII}} = -\sigma^{-1} \int_{2\theta}^{\beta_p} B^{VII1}(\alpha_p, \beta) F_C d\beta;$$

$$V_k^{\mathrm{VIII}} = 1.363841418 V_0.$$

The total volume of the compression reinforcing bar is V_C= $18.31238360V_0$.

The total volume of the reinforcing bars is V_K= $43.70120157V_0$.

The total volume of the material used for the structure is V=V_S+V_K=$97.86472194V_0$.

The same volume computed by the alternative formula (I.2.12) is V=$97.86471582V_0$.

6 Final remarks

The analyses of concrete examples of Michell cantilevers presented in the paper show complexity of the emerging internal force fields and the density of fibres. Equivalence of the formulae for the optimal weight (I.2.6 and I.2.12) is proven analytically or, in more complicated cases, by numerical integration of the analytical formulae. The paper shows by examples that the static problems of Michell structures can be approximated by static problems of specific statically determinate trusses with finite number of joints with arbitrary accuracy. This property of the Michell structures can be proven mathematically. It is sufficient to rearrange the equilibrium equations (III.2.4) to their variational form

$$\iint \left[T_1\left(\frac{\partial \overline{u}}{\partial \alpha} + \overline{v}\right) + T_2\left(\frac{\partial \overline{v}}{\partial \beta} + \overline{u}\right)\right] d\alpha d\beta = f(\overline{u}, \overline{v}) \forall\, \overline{u}, \quad \overline{v} \text{ kinematically admissible,} \tag{6.1}$$

where $f(.,.)$ is a linear form representing the virtual work of the loading and the integration extends over admissible values of parameters. The above variational equation, possibly augmented with boundary integrals as in (I.2.5), can be obtained from the conditions of equilibrium of approximating trusses

$$\sum_{\text{tension members}} N_K \overline{\Delta}_K + \sum_{\text{compression members}} N_K \overline{\Delta}_K = \mathbf{Q}^T \overline{\mathbf{q}} \quad \forall\, \overline{\mathbf{q}} \in R^{\mathrm{n}}; \tag{6.2}$$

by appropriate passage to the limit: $n \rightarrow \infty$. Here, K indexes the members, N_K are longitudinal forces in the members, $\overline{\Delta}_K = \Delta_K(\overline{\mathbf{q}})$ are elongations of members associated with virtual displacements of nodes $\overline{\mathbf{q}}$ and $\mathbf{Q}$ represents the column of the point loads applied at the nodes. The passage from (6.2) to (6.1) can also be performed in the case of the simply supported beam of Michell, which confirms the recent analytical result by Zhou and Li (2004).

The plane Michell cantilevers, subjected to point loads, are reinforced by bars of finite cross sections. By analogy, possible spatial Michell structures should be reinforced by membrane coatings if subjected to line loadings and, additionally, by reinforcing cables (i.e. bars with no bending) if subjected to point loads. Consequently, the optimal designs will comprise all possible structures developed in structural mechanics: special composites, membrane shells and cables, capable of transmitting stresses without shearing. Let us cherish our hope here that these questions will be cleared up in the near future.

Acknowledgement The project had been suggested by Prof. George Rozvany. His friendly encouragement is highly acknowledged.

References

Chan HSY (1967) Half-plane slip-line fields and Michell structures. Q J Mech Appl Math 20:453–469

Gilbert M, Darwich W, Tyas A, Shepherd P (2005) Application of large-scale optimization techniques in structural engineering practice (CD ROM, in print). 6th world congress of structural and multidisciplinary optimization, Rio de Janeiro, 30 May–03 June 2005

Graczykowski C, Lewiński T (2005) The lightest plane structures of a bounded stress level, transmitting a point load to a circular support. Control Cybern 34:227–253

Graczykowski C, Lewiński T (2006a) Michell cantilevers constructed within trapezoidal domains—Part I: geometry of Hencky nets. Struct Multidisc Optim (in press)

Graczykowski C, Lewiński T (2006b) Michell cantilevers constructed within trapezoidal domains—Part II: virtual displacement fields. Struct Multidisc Optim (in press)

Graczykowski C, Lewiński T (2006c) Michell cantilevers constructed within trapezoidal domains—Part III: force fields. Struct Multidisc Optim (in press)

Hemp WS (1973) Optimum structures. Clarendon, Oxford

Lewiński T (2004) Michell structures formed on surfaces of revolution. Struct Multidisc Optim 28:20–30

Lewiński T, Zhou M, Rozvany GIN (1994a) Extended exact solutions for least-weight truss layouts—Part I: cantilever with a horizontal axis of symmetry. Int J Mech Sci 36:375–398

Lewiński T, Zhou M, Rozvany GIN (1994b) Extended exact solutions for least-weight truss layouts—Part II: unsymmetric cantilevers. Int J Mech Sci 399–419

Prager W (1978a) Nearly optimal design of trusses. Comput Struct 8:451–454

Prager W (1978b) Optimal layout of trusses of finite number of joints. J Mech Phys Solids 26:241–250

Zhou K, Li J (2004) The exact weight of discretized Michell trusses for a central point load. Struct Multidisc Optim 28:69–72